# SIMULATION AND FABRICATION OF Ag/ZnO-NANORODS/Ag ULTRAVIOLET DETECTORS ON *p*-TYPE SILICON

M. KUMAR[a], S. SINGH[a], P. K. TIWARI[b], S.H. PARK[a,*]
[a]*Department of Electronic Engineering, Yeungnam University, Gyeongsan-si, Gyeongsangbuk-do, South Korea*
[b]*Department of Electrical Engineering, Indian Institute of Technology, Patna, India*

Hydrothermal method was successfully utilized to grow ZnO-nanorods on *p*-type silicon substrate. The highly dense grown ZnO-nanorods are well-aligned, and perpendicularly to substrate confirmed by scanning electron microscopy. The X-ray diffraction analysis confirmed that the [002] orientation was the major growth direction of the ZnO nanorods. A shadow masks have used to fabricate Metal–semiconductor–metal (MSM) structure. Three arrays of Ag interdigitated electrodes were then deposited onto the ZnO-nanorod/Si substrates. The current characteristics of [Ag/ZnO-nanorod/Ag]/Si devices were investigated range of -2 to +2 V. The as-fabricated devices showed a contrast ratio (i.e., the photocurrent/dark current) of 1.17 along with room temperature 0.115 mA/W responsivity at 365 nm and -2 V. A simulation analysis for the theoretical MSM structure has also been done in this work. A Visual TCAD was also used to simulate this device. A comparative study of experimentally and theoretically obtained results was also carried out and both results were found in good agreement of each other.

(Received September 4, 2019; Accepted February 4, 2020)

Keywords: ZnO; Hydrothermal, Silver; Interdigitated electrodes, UV-detectors, Simulation

## 1. Introduction

Ultraviolet (UV) detectors are applied in the areas of water purification, currency counting, chemical analysis, optical communications, ozone layer detection, biological analysis, missile warning systems, astronomical studies, flame sensing, etc. [1,2]. Wide-bandgap materials such as diamond ($E_g \approx 5.45$ eV), SiC ($E_g \approx 3.26$ eV), GaN ($E_g \approx 3.45$ eV), and ZnO ($E_g \approx 3.26$ eV) have been used by various research groups for fabricating UV-detectors [3]. In the recent past, ZnO in particular has drawn much attention in comparison to GaN and SiC-based UV-detectors [4-6] because GaN and SiC are less compatible with other semiconductors in comparison to ZnO [7]. Hence, most research groups are focusing on ZnO because of this compatibility and because it is a low-cost and environment friendly material [8-10]. It shows much high exciton binding energy in compare to competitive III-V group material system, which could be useful for UV detection applications. In recent years, quantum confined nanostructures of ZnO such as nanobelts [11], nanowires [12], nanotubes [13], nanorings [14], nanorods [15, 16], nanobows [14], nanospheres [17], nanoribbons [18], etc. have attracted great interest. Recently, ZnO nanostructures showed better UV sensing properties than ZnO thin films [19] because of larger surface-to-volume ratio, which increases UV light absorption and thus increases the response under UV exposure [20]. Various types of 1D ZnO nanostructure devices have been reported in the past, including chemical sensors [21], nano lasers [22], light emitting diodes [23], photodetectors [24], field effect transistors [25], photovoltaic devices [26], etc. ZnO-nanorods and nanowires have received particular attention, and numerous studies reported on ZnO-nanorod and nanowire-based devices with many electronic and optoelectronics application [27-30]. In the past few decades, many methods for preparing ZnO nanorods have been reported, such as electrodeposition [31], sol gel technique [32], chemical vapor deposition [33], and hydrothermal [15, 16, 34] and vapor–liquid–

* Corresponding author: sihyun_park@ynu.ac.kr

solid methods [35]. The hydrothermal technique delivers numerous rewards in contrast to the supplementary methods, such as low cost, large-scale deposition, and possible control of the morphology of the resulting films in form of rough deposition to well-aligned nanorods [15, 16, 34].

In this study, we fabricated hydrothermal ZnO nanorod-based MSM UV-detectors with Ag metal contacts on Si substrates. Up to now, most of the research focused on Au, Au/Ti, Au/Cr, and Al metals for their MSM UV-detectors; however, reports on Ag metal-based MSM ultraviolet-detectors are limited. Vasudevan *et al.* reported the fabrication of ZnO-nanorods based MSM ultraviolet-detectors with Au metal electrodes. They grew ZnO nanorods on ZnO seed/$SiO_2$/Si samples by a solution-based hydrolysis method [36]. Ko *et al.* reported the fabrication of Au/Ti-based MSM UV-detectors on hydrothermally grown ZnO nanorods [37]. Mamat *et al.* used Al contact electrodes to fabricate MSM ZnO nanorod ultraviolet-detectors [38]. Similarly, some reports of MSM ultraviolet-detectors with Ag metal are also available. Ji *et al.* compared the parameters of Ag metal-based MSM ultraviolet-detectors fabricated using ZnO thin films and ZnO nanorods [39]. Chen *et al.* used Ag/Au contacts to fabricate MSM ZnO nanorod ultraviolet-detectors [40]. Reported research have focused mainly on the lithography technique for designing MSM electrodes.

Although various groups have reported on fabrication of ZnO nanorod-based MSM ultraviolet-detectors in the past [36-40], but no report is available on simulation study of ZnO nanorod-based MSM ultraviolet-detectors. In the present work, we have done theoretical simulation for the MSM UV detectors and we have also presented experimental results. We have used a less-expensive shadow mask technique for the deposition of MSM metal electrodes. Hence, our less complicated and more economical method could be better for fabricating ZnO nanorod-based MSM ultraviolet-detectors for optoelectronic applications.

## 2. Methods and materials

### 2.1. ZnO nanorod deposition

The *p*-type Si substrates were cut to 1.5 in. × 1.5 in. samples using a diamond cutter. After shaping the substrate, it was successively cleaned with acetone and methanol in an ultrasonic bath, as shown in Figs. 1(a) and (b). The Si substrates were then dipped many times in deionized (DI) water and dried with blowing $N_2$. The cleaned Si substrates were then subjected to seed-layer deposition. Zinc acetate dehydrate was added to ethyl alcohol to form a 60 mM solution. A seed layer of 50-nm-thick ZnO was deposited onto the Si substrates by dipping method into the seed-layer solution, as shown in Fig. 1(d). For growth of the ZnO-nanorods, zinc nitrate hexahydrate and hexamethylenetetramine (HMT) were added to DI water to form a 30 mM solution. The ZnO/Si samples were dipped into this solution to grow the ZnO-nanorods, as shown in Fig. 1(e). After the deposition of the ZnO nanorods, the substrates were rinsed numerous times with DI water to eliminate any unused precursor particles. All the chemicals were used without further purification. Details of hydrothermal method for ZnO-nanorods growth might be available elsewhere [15, 16].

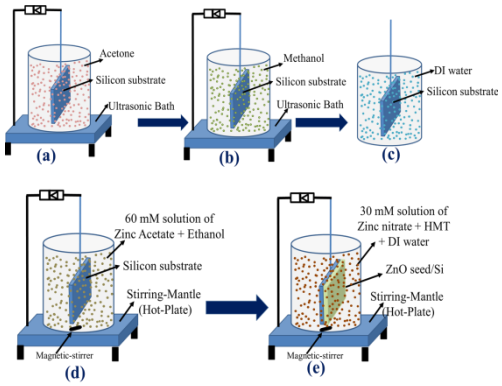


*Fig. 1. (a)–(e) Schematic drawing for various stages of ZnO-nanorods deposition.*

### 2.2. ZnO-nanorod UV-detector fabrication

ZnO-nanorod MSM based ultraviolet-detectors were fabricated using Ag metal. Interdigitated Ag contacts (IDCs) were deposited onto the ZnO-nanorod/Si substrates by thermal evaporation. A shadow mask consisting of three IDC arrays was used for Ag deposition. In this work, IDCs with six fingers were used; the spacing and width of the fingers were both 0.3 mm. A schematic of the [Ag/ZnO- nanorod/Ag]/Si device under UV light ($\lambda$ = 0.365 μm; $P$ = 650 μW) is shown in Fig. 2(a). The dimensions of the IDC are shown in Fig. 2(b).

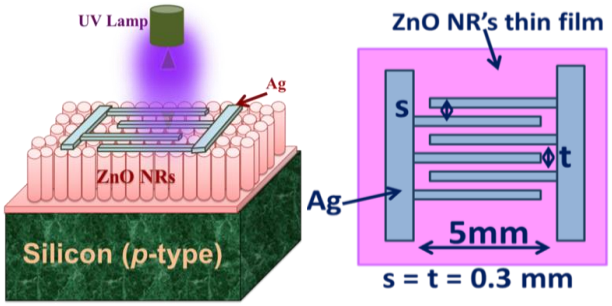


*(a)* *(b)*

*Fig. 2. [Ag/ZnO-nanorod/Ag]/Si detector (a) Schematic diagram, (b) top view of metal electrodes.*

### 2.3. Experiential characterization

Surface morphology was surveyed by scanning electron microscopy. The crystallography examined by X-ray diffraction. ZnO nonorods thickness was measured using an ellipsometer. A UV lamp with a wavelength of 365 nm with 650 μW power was used as the light source. *I–V* characteristics was analyzed by Agilent parameter analyzer.

## 3. Results and discussion

### 3.1. Structural properties

The SEM micrographs for the ZnO-nanorods are shown in Fig. 3. It can be seen from the figure that the density of the ZnO-nanorods was high and their growth was well aligned and perpendicular to the Si substrate. The length and diameter of the ZnO-nanorods were obtained from the SEM micrograph and were found to be 45 μm and 1.20 μm, respectively [41].

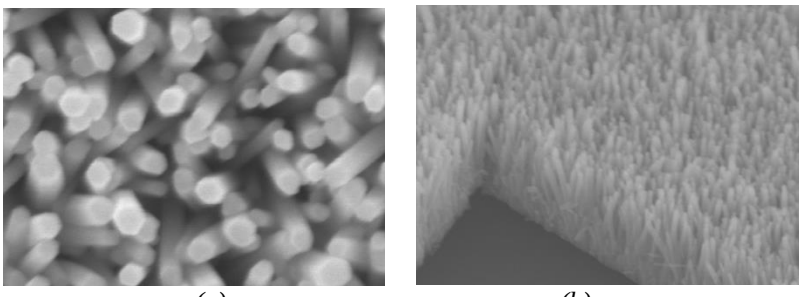

*(a)* *(b)*

*Fig. 3. ZnO-nanoraods grown by hydrothermal method (a) Top view; (b) cross sectional view.*

The thickness of ZnO-nanorods determined using an ellipsometer were strongly correlated with the findings from the cross-sectional view of SEM micrograph. X-ray diffraction pattern of the ZnO-nanorods is shown in Fig. 4. It indicated various peaks at 2$\theta$ diffraction angles of 31.76°, 34.46°, 36.32°, 47.59°, and 72.68°. We mainly consider here the main peaks associated with ZnO,

which correspond to the (100), (002), and (101) planes. All X-ray diffraction features were in good accordance with JCPDS card No. 36-1451 [41]. The (002) crystallographic plane shows 0.3542 full-width at half maximum along with the 2.60244 Å *d*-spacing at $2\theta = 34.46°$ [41].

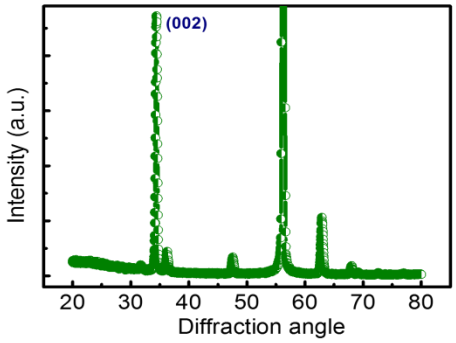


*Fig. 4. X-ray diffraction of ZnO-nanorods.*

### 3.2. Simulation study for [Ag/ZnO- nanorod/Ag]/Si based UV-detectors

The present structure is numerically simulated using Visual TCAD of Cogenda International [42]. To simulate the structure, drift-diffusion model of carrier transport [42], analytic mobility model [42], SRH [42], Auger and direct recombination models [42] and optical generation model [42] are activated. ZnO default model parameters available in Visual TCAD library are also activated.

In order to minimize the simulation time, the present structure is scaled down in nanometer regime. The overall device dimensions are 50nm×50nm ×50nm. The ZnO layer is considered to be grown on a silicon film of dimension 50nm×50nm ×20nm. The ZnO film (50nm×50nm ×30nm) is considered with the doping concentration of $10^{18}$ $cm^{-3}$. Silver (Ag) is used to create anode and cathode contacts in order to form a MSM contact, as shown in Fig. 5. Both contact fingers width and spacing are considered to be 3nm, whereas the separation between finger bases is 5nm. The metal semiconductor contacts are considered to be ideal with negligible interface trap density.

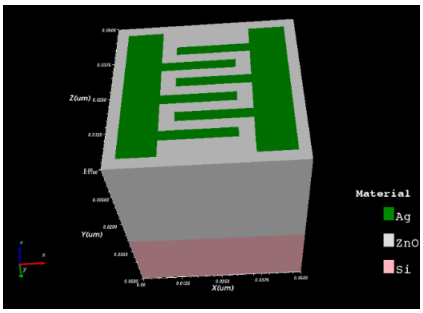


*Fig. 5. Schematic diagram of device, obtained from simulation.*

### 3.3. Electrical properties

To examine the UV light response on [Ag/ZnO-nanorod/Ag]/Si devices, current-to-voltage measurements were performed. The obtained *I–V* curve in the dark and under UV light is displayed in Fig. 6. It is seen that under UV illumination, the current increased from $6.38\times10^{-8}$ to $7.48\times10^{-8}$A. The standard equation for the Ag/ZnO-nanorod contact might be explained as [41, 43]

$$I = I_0 e^{\left(\frac{qV}{nkT}-1\right)} \quad (1)$$

Where $I_0$ is the saturation current, $q$ is the charge of the electron, $V$ is the voltage, $k$ is the Boltzmann constant, $T$ is the temperature in Kelvin, and $n$ is the ideality factor. The saturation current can be expressed by the following equation:

$$I_0 = AA^*T^2e^{\left(-\frac{q\emptyset_B}{kT}\right)} \quad (2)$$

where $A$ is the area of contact, $A^*$ is Richardson's constant, which has a value of ~32 $cm^{-2}$ $K^{-2}$, and $\emptyset_B$ is the barrier height [41,43].

Fig. 7 presented the logarithmic scale current characteristics of MSM based [Ag/ZnO-nanorod/Ag]/Si devices in the dark and under ultraviolet light. It can be seen that the trend of dark current and ultraviolet current for our devices showed similar trends, as reported by others [39, 40]. A comparative study of past reported results and our results on ZnO based UV-detectors is summarized in the Table 1. Some groups have fabricated metal contacts with shadow-mask technique while some groups have used shadow-mask for depositing their metal-contacts. Chen *et al.* reported Ag-Au/ZnO nanorod MSM on flexible polyimide substrate by aqueous method. They have deposited interdigited Ag-Au metal contacts by photolithography process [20]. Similarly Ji et al., Huang *et al.* and He *et al.*, have used photolithography process for depositing interdigited metal electrodes for their ZnO based MSM UV-detectors [39-47]. Some research groups like Wang *et al.*, Kashif *et al.* and Ko *et al.* have used shadow-mask technique for depositing interdigited metal contacts for their UV detectors [43-48]. Mainly all of these have used applied bias in the range of 3V to 10V, which are tabulated in Table 2. In our case we have got promising results in low voltage range of -2 to +2 V.

In Fig. 7 shows simulated current characteristics under dark and illuminant conditions, which was compared experimental findings. To compare the outcomes the simulation current is normalized against the dimensions. However, as the simulation is done under the ideal condition and the dimensional normalization is very crude, the simulation result is deviated by the experimental one.

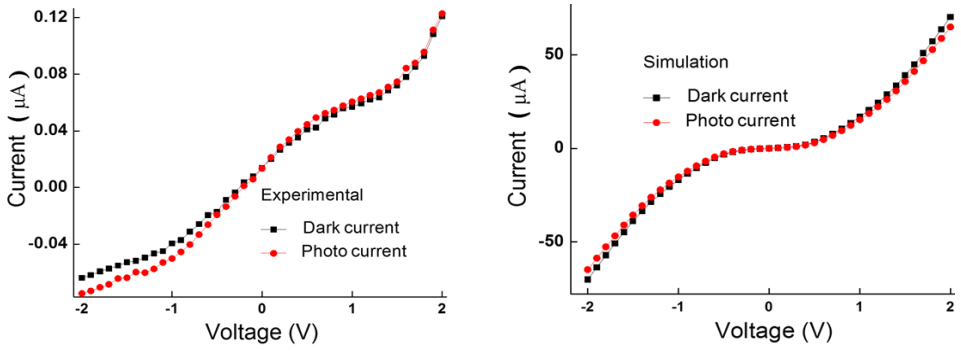


*Fig. 6. Linear I-V characteristics of [Ag/ZnO-nanorods/Ag]/Si detector, measured under UV and dark light.*

*Table 1. Detector Parameters for UV-Detection*

| Sr. Num. | Photodetector parameters | [Ag/ZnO-nanorods/Ag] MSM UV-Detectors on Si |
|---|---|---|
| 1. | Dark-current (A) (at V= -2.0 V) | $6.38\times10^{-8}$ |
| 2. | UV-current (A) (at V = -2.0 V) | $7.48\times10^{-8}$ |
| 3. | Contrast ratio | 1.17 |
| 4. | Responsivity (mA/W) | 0.115 |

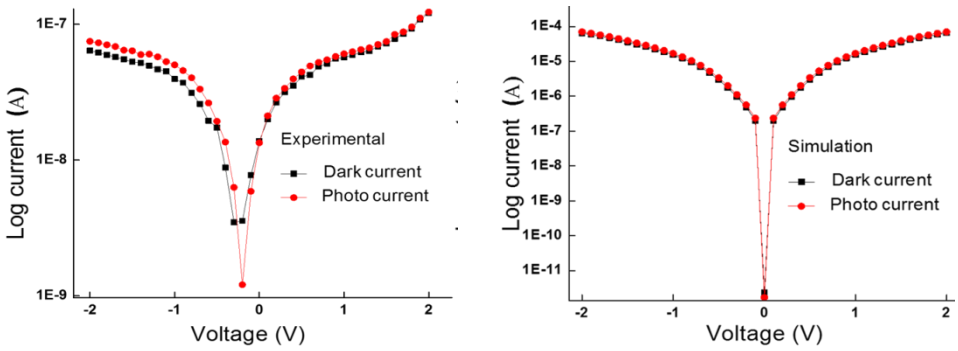


*Fig. 7. Log Scale current characteristics for [Ag/ZnO-nanorods/Ag]/Si detector, measured under illumination as well as dark light.*

Under UV illumination, the conductivity of the devices increased drastically with the electron–hole pair generation under UV light and oxygen adsorption on the surfaces of the ZnO-nanorods [44, 45]. This photoconduction mechanism of the ZnO- nanorod detectors were explained here in more elaborative way. Photoresponse of ZnO-nanorods is mostly governed through the process of oxygen molecule's adsorption and desorption on the surface. Under dark conditions, $O_2$ captures free electrons from the surfaces of the ZnO-nanorods, leading to adsorbed $O_2$.

$$O_2\,(g) + e^- \rightarrow O^{-2}\,(ads) \tag{3}$$

This adsorption decreases the conductivity and creates a depletion region near the surfaces of the ZnO- nanorods. Under UV light illumination, photons with an energy $h\upsilon > E_g$ (the bandgap energy) fall on the surface of the ZnO-nanorod, generating e–h pairs.

$$(h\upsilon \rightarrow e^- + h^+) \tag{4}$$

The holes move towards the surfaces of the nanorods and interact with the adsorbed oxygen.

$$h^+ + O^{-2}\,(ads) \rightarrow O^2\,(g) \tag{5}$$

This phenomenon causes a decrease in the depletion layer and an increase in the conductivity, which leads to an increase in the photocurrent [44-48].

*Table 2. A comparative study of characteristics of ZnO-NR UV-detector, fabricated with lithography-process and shadow-mask methods.*

| | **Method of ZnO deposition** | **Geometry of UV-detectors** | **Method of metal deposition** | **Applied Voltage** | **Dark-current (A)** | **Photo-current (A)** | **Contrast ratio** | **Responsivity (mA/W)** | **Ref.** |
|---|---|---|---|---|---|---|---|---|---|
| 1. | Hydrothermal | Ag/ZnO/Ag nanorod MSM on Si substrates | Shadow-mask | -2.0 | $6.38\times10^{-8}$ | $7.48\times10^{-8}$ | 1.17 | 0.115 | This study |
| 2. | RF sputtering and aqueous solution method | Ag-Au/ZnO nanorod MSM on flexible polyimide substrate | Photolithography process | 5V | ~ $10^{-7}$A | - | - | $10^{2}$ at 360 nm | [20] |
| 3. | Chemical solution method | Ag/ZnO nanorod MSM structure on glass substrates | Photolithography process | 5V | 60.3 nA | 0.18 mA | 200 | 41.22 | [39] |
| 4. | RF magnetron sputtering | Ag/ZnO on single crystal Si with thin film | Shadow-mask | 3V | 24.19mA | 32.8mA | 1.35 | - | [46] |
| 5. | Chemical solution method | Ag/ZnO MSM structure with thin film on glass substrates | Photolithography process | 5V | 3.55 nA | 552 nA | 155 | 0.13 | [39] |
| 6. | RF magnetron sputtering | Ag/ZnO MSM structure with thin film on $SiO_2$/n- Si | Photolithography process | 5V | $6\times10^{-7}$ | $3.7\times10^{-5}$ | - | - | [47] |
| 7. | Sol-gel method | Ag/ZnO nanorod MSM structure on $SiO_2$/p- Si | Shadow-mask | 3V | $4.46\times10^{-6}$ | $2.23\times10^{-5}$ | - | - | [41] |
| 8. | Hydrothermal | Ti/Au/ZnO nanorod MSM structure on $SiO_2$/Si | Shadow-mask And Photolithography | 10V | - | $1.91\times10^{-4}$ | 37.4 | - | [37] |
| 9. | Hot-solution-phase method | Glass/Ag/ZnO seed layer/ZnO nanowires | Photolithography | 5V | $0.52\times10^{-6}$ | $0.6\times10^{-3}$ | - | - | [45] |

## 4. Conclusions

In summary, we report the fabrication of MSM UV-detectors using highly dense ZnO-nanorods on *p*-type Si <100> substrates. The growth of ZnO-nanorods was take place on the 50-nm seed layer of ZnO/Si substrate through hydrothermal technique. Systematically analysis of ZnO-nanorods has been gone through by SEM and x-ray diffractometer. Results indicate that ZnO-nanorods exhibited high crystallinity with a hexagonal wurtzite lattice. The fabricated [Ag/ZnO-nanorod/Ag]/Si detectors showed good performance under UV illumination (365 nm and 650 µW).

The responsivity and contrast ratio were found to be 0.115 mA/W and 1.17, respectively, at -2.0 V bias. A simulation study of [Ag/ZnO-nanorod/Ag]/Si structure was also done with help of visual TCAD software. The simulated data showed similar trend of dark and photo current as the experimental data. The proposed method is a less-complex and low-cost technique for fabricating nanoscale photodetectors for optoelectronic applications.

**Acknowledgments**

The authors gratefully acknowledge Prof. Satyabrata Jit for allowing use of the research facility at the Department of Electronics Engineering, Indian Institute of Technology, BHU, Varanasi, India.

## References

[1] L. Sang, M. Liao, M. Sumiya, Sensors **13,** 10482 (2013).
[2] H. Chen, K. Liu, L. Hu, A. A. Al-Ghamdi, X. Fang, Mater Today **18,** 493 (2015).
[3] J. Millán, P. Godignon, A. P. Tomás, Automatika **53**, 107 (2012).
[4] S. Singh, S. H. Park, Superlattices Microstruct. **86**, 412 (2015).
[5] N. K. Reddy, M. Devika, K. R. Gunasekhar, E. S. R. Gopal, NANO **11**, 1650077 (2016).
[6] Q. Wang, Q. Yu, J. Liu, T. Ai, H. Li, NANO **10**, 1550083 (2015).
[7] D. Klimm, IUCrJ. **1**, 281 (2014).
[8] S. Singh, S. H. Park, J. Nanosci. Nanotechnol. **16**, 861 (2016).
[9] S. Singh, P. Chakrabarti, J. Nanosci. Nanotechnol. **14**, 3552 (2014).
[10] S. Singh, P. Chakrabarti, J. Nanosci. Nanotechnol. **12**, 1880 (2012).
[11] Y. Ding, Y. Liu, S. Niu, W. Wu, and Z. L. Wang, J. Appl. Phys. **116**(1), 154304 (2014).
[12] M. A. Zimmler, F. Capasso, S. Müller and C. Ronning, Semicond. Sci. Technol. **25**(1), 024001 (2010).
[13] T. İpeksaç, F. Kaya and C. Kaya, Mater. Lett. **100**, 11 (2013).
[14] W. L. Hughes, Z. L. Wang, Appl. Phys. Lett. **86**(1), 043106 (2005).
[15] S. Singh, S. H. Park, Korean J. Met. Mater. **54**, 347 (2016).
[16] S. Singh, G. R. Dillip, S. Vyas, M. R. Hasan, I. K. Park, P. Chakrabarti, S. H. Park, Microsys. Technol. **1**, (2015).
[17] C. Yang, Q. Li, L. Tang, A. Bai, H. Song, Y. Yu, J. Mater. Sci. **51**, 5445 (2016).
[18] M. E. Kilic, S. Erkoc, Curr. Appl. Phys. **14**, 57 (2014).
[19] L. W. Ji, S. M. Peng, Y. K. Su, S. J. Young, C. Z. Wu, W. B. Cheng, Appl. Phys. Lett. **94**(1), 203106 (2009).
[20] T. P. Chen, S. J. Young, S. J. Chang, C. H. Hsiao, Y. J. Hsu, Nanoscale Res. Lett. **7**, 1 (2012).
[21] S. Ameen, D. R. Parka, M. S. Akhtar, H. S. Shin, Mater. Lett. **164**, 562 (2016).
[22] Y. H. Chou, B. T. Chou, C. K. Chiang, Y. Y. Lai, C. T. Yang, H. Li, T. R. Lin, C. C. Lin, H. C. Kuo, S. C. Wang, and T. C. Lu, ACS Nano **9**, 3978 (2015).
[23] M. A. Abbasi, Z. H. Ibupoto, M. Hussain, O. Nur, M. Willander, Nanoscale Res. Lett. **8**, 1 (2013).
[24] B. O. Jung, D. C. Kim, B. H. Kong, D. W. Kim, H. K. Cho, Sensor Actuat B-Chem **160**, 740 (2011).
[25] P. Y. Yang, J. L. Wang, P. C. Chiu, J. C. Chou, C. W. Chen, H. H. Li, H. C. Cheng, IEEE Electr Device L **32**, 1603 (2011).
[26] N. K. Reddy, M. Devika, K. R. Gunasekhar, E. S. R. Gopal, Nano **11**(1), 1650077 (2016).
[27] Y. Qiu, H. Zhang, L. Hu, D. Yang, L. Wang, B. Wang, J. Ji, G. Liu, X. Liu, J. Lin, F. Li, S. Han, Nanoscale **4**, 6568 (2012).
[28] B. H. Chu, B. S. Kang, F. Ren, C. Y. Chang, Y. L. Wang, S. J. Pearton, A. V. Glushakov, D. M. Dennis, J. W. Johnson, P. Rajagopal, J. C. Roberts, E. L. Piner, K. J. Linthicum, Appl. Phys. Lett. **93**(1), 042114 (2008).
[29] M. A. Zimmler, F. Capasso, S. Müller, C. Ronning, Semicond. Sci. Technol. **25**, 024001 (2010).
[30] A. Bhattacharya, V. P. Rao, C. Jain, A. Ghose, S. Banerjee, Mater. Lett. **117**, 128 (2014).
[31] M. Skompska, K. Zarebska, Electrochim. Acta **127**, 467 (2014).
[32] K. L. Foo, U. Hashim, K. Muhammad, C. H. Voon, Nanoscale Research Letters **9**(1), 429 (2014).
[33] R. R. Zhao, X. Q. Wei, M. Ding, X. J. Xu, Sci. Adv. Mater. **6**, 500 (2014).
[34] Y. Liu, G. Liu, Y. Wang, W. Gao, H. Hao, B. Huang, Nano **11**, 1650024 (2016).

[35] Q. X. Zhao, P. Klason, M. Willander, Appl. Phys. A **88**, 27 (2007).
[36] A. Vasudevan, S. Jung, T. Ji, IEEE Sens. J **12**, 1317 (2012).
[37] Y. H. Ko, G. Nagaraju and J. S. Yu, Nanoscale Res. Lett. **10**, 1 (2015).
[38] M. H. Mamat, Z. Khusaimi, M. M. Zahidi, M. R. Mahmood, Jpn. J. Appl. Phys. **50**(1), 06GF05 (2011).
[39] L. W. Ji, C. Z. Wu, T. H. Fang, S. M. Peng, S. J. Young, W. Water, T. H. Meen, C. H. Liu, J. Nanoelectron. Opt. **5**, 300 (2010).
[40] T. P. Chen, S. J. Young, S. J. Chang, C. H. Hsiao, Y. J. Hsu, Nanoscale Res. Lett. **7**(1), 214 (2012).
[41] M. Kashif, U. Hashim, M. E. Ali, K. L. Foo, M. U. Ali, J. Nanomater. **1**, (2013).
[42] Visual TCAD reference manual, Genius, 3-D Device Simulator, Version 1.9.0, Cogenda Pte Ltd, Singapore (2008).
[43] N. K. Hassan, M. R. Hashim, K. A. Heuseen, N. K. Allam, Chem. Phys. Lett. **604**, 22 (2014).
[44] G. M. Ali, P. Chakrabarti, J. Phys. D: Appl. Phys. **43**(1), 415103 (2010).
[45] D. Somvanshi, A. Pandey, S. Jit, J. Nanoelectron. Opt. **8**, 349 (2013).
[46] Y. He, W. Zhang, S. Zhang, X. Kang, W. Peng, Y. Xu, Sens. Actuators A **181**, 6 (2012).
[47] C. Wang, D. Wang, C. Pang, X. Wang, J. Yin, H. Zhao, 2012 Int. Conf. IEEE Measurement, Information and Control (MIC) **2**, 659 (2012).
[48] B. Huang, G. He, Y. Wu, L. Zhang, J. Li, D. Guo, S. Wu, in Proc. SPIE 6722, 3rd Int. Symp. Advanced Optical Manufacturing and Testing Technologies: Advanced Optical Manufacturing Technologies, 67221W (2007).